

# Chapter 10

## Dropwise Condensation of Bismuth on Horizontal and Vertical Surfaces



Praveen Somwanshi, K. Muralidhar, and Sameer Khandekar

### Nomenclature

$A$	Surface area, $m^2$
$C_p$	Specific heat of condensate at constant pressure, $J/kgK$
$h$	Heat transfer coefficient, $q''/(T_{sat} - T_w)$ , $W/m^2K$
$h_{int}$	Interfacial heat transfer coefficient, $W/m^2K$
$h_{lv}$	Latent heat of vaporization, $J/kg$
$k$	Thermal conductivity of condensate, $W/mK$
$k_{coat}$	Thermal conductivity of coating, $W/mK$
$m_{avg}$	Mass of the condensate averaged over space and time, $kg$
$M$	Molecular weight, $kg/kmol$
$N$	Nucleation site density, $cm^{-2}$
$p$	Pressure, $N/m^2$
$q$	Surface heat transfer, $W$
$q''$	Surface heat flux, $W/m^2$
$r_{avg}$	Radius of drop averaged over space and time, $m$
$r_b$	Base radius of drop, $m$
$r_{crit}$	Radius of drop at instability due to slide-off, $m$
$r_{max}$	Radius of drop at instability due to fall-off, $m$
$r_{min}$	Minimum radius of the thermodynamically stable drop, $m$
$R$	Base radius of coalesced drop under equilibrium conditions, $m$
$R_{avg}$	Base radius of drop averaged over space and time, $m$
$t$	Time, $s$ ; suffix IS is inertia-surface tension; IV is inertia-viscous; VS is viscous-surface tension
$\Delta t$	Time step, $s$
$T_{avg}$	Average temperature of condensation = $(T_{sat} + T_w)/2$

$T_{\text{sat}}$	Saturation temperature in vapor phase, K
$T_w$	Substrate temperature, K
$\Delta T$	Degree of subcooling, $(T_{\text{sat}} - T_w)$ , K
$U$	Terminal velocity of sliding drop or relative velocity between the wall and sliding drop; also characteristic velocity of drop coalescence, m/s
$v_l, v_v$	Specific volume, $\text{m}^3$ ; $l$ for liquid and $v$ for vapor
$V$	Volume of liquid drop, $\text{m}^3$

## Dimensionless Quantities

Bo	Bond number, $\frac{\rho g R^2}{\sigma}$
$C_f, \overline{C}_f$	Local and surface-averaged skin friction coefficient, $\tau_w / (1/2)\rho U^2$
Fr	Froude number, $\frac{U^2}{gR}$
$(\text{Nu})_{\text{sd}}$	Local Nusselt number of single sliding drop, $h r_b / k$
Oh	Ohnesorge number, $\frac{\mu}{\sqrt{\rho R \sigma}}$
Pr	Prandtl number, $\mu C_p / k$
Re	Reynolds number, $\rho UR / \mu$
We	Weber number, $\frac{\rho U^2 R}{\sigma}$

## Greek Symbols

$\alpha$	Inclination angle, radians
$\mu$	Dynamic viscosity of liquid phase, Pa-s
$\rho$	Liquid density, $\text{kg}/\text{m}^3$ ; $l$ for liquid and $v$ for vapor
$\sigma$	Surface tension coefficient at liquid-vapor interface, N/m
$\tau_w, \overline{\tau}_w$	Local and average wall shear stresses, $\text{N}/\text{m}^2$
$\theta$	Contact angle, degrees
$\theta_{\text{adv}}$	Advancing contact angle, degrees
$\theta_{\text{rcd}}$	Receding contact angle, degrees
$\Delta\theta$	Contact angle hysteresis, $(\theta_{\text{adv}} - \theta_{\text{rcd}})$ , degrees
$\theta_{\text{avg}}$	Average contact angle, $^\circ$

## 10.1 Introduction

As discussed in Chaps. 5–7, condensation occurs on a solid wall when the surface temperature falls below the local saturation temperature of the adjoining mass of vapor. On specially treated surfaces, liquid droplets will appear at specific nucleation sites. As the phase change process proceeds, these droplets grow by direct condensation from the vapor phase, coalesce with neighboring drops, and may fall off or

start to slide down the substrate. The process is cyclic and drop instability will prevent the formation of a liquid film. Such a phase change process, termed dropwise condensation (Carey 2008), is heterogeneous. Vapor condenses in the form of discrete liquid drops on or underneath a cold solid substrate.

Dropwise condensation can be sustained only on specially textured surfaces (Rose 2002; Vemuri and Kim 2006; Rausch et al. 2008). The heat transfer coefficient during dropwise condensation can be quite high, for example, up to 30 times greater than the filmwise mode, when tested with Langmuir-Blodgett surfaces (Rose 2002) and 5–20 times better when a promoter layer is used (Koch et al. 1998a, b). Leaching of the coated or textured substrate can alter its wettability characteristics and result in its aging. Hence, apart from heat fluxes, it is important to estimate wall shear stresses created during drop movement.

Drops are expected to form at individual nucleation sites, while the area between the drops remains inactive with respect to condensation (Leach et al. 2006). The diameter of the smallest drop at nucleation can be estimated from thermodynamic considerations (Carey 2008). Subsequently, the drop grows by direct condensation at a rate determined by the conduction resistance through the drop, interfacial heat transfer coefficient, and the available temperature difference. Larger drops also grow by coalescence with their neighbors. When a certain size is reached, drops become gravitationally unstable, fall off, or slide along the surface, wiping other drops along their path. Fresh nucleation sites are thus revealed, and the condensation process repeats in a cyclic manner.

A multiscale dropwise condensation model, starting from the atomic scale, progressing towards the growth of droplets, coalescence, and drop instability has been reported by various authors (Rose 2002; Vemuri and Kim 2006; Rausch et al. 2008) for condensation of water vapor. The model developed by the authors, as described in Chap. 6, is comprehensive and the deformed drop shape is determined by the two-circle approximation. In addition, the process of coalescence is taken to be instantaneous.

In this chapter, the original model is extended by including the characteristics of coalescence of the droplets. While condensation of bismuth is the primary focus, results for water are also generated for comparative purpose. The effect of drop coalescence on wall shear stress and heat transfer rates in dropwise condensation is determined. In addition, the mathematical model is parallelized using MPI to run for large surface areas on a high-performance computing system.

The choice of bismuth as the working fluid is motivated by the range of applications where liquid metals are encountered. These include the use of liquid sodium in fast breeder reactors and in distillation processes required to produce high purity precious metals such as gold. Thermophysical properties of bismuth and water at the selected saturation pressure and temperature are given in Table 10.1. Density of water is substantially smaller than bismuth; it has higher latent heat of vaporization, lower surface tension and viscosity. Thermal conductivity of bismuth is substantially higher than that of water, thus giving rise to a small Prandtl number. Differences in thermophysical properties lead to significant changes in the drop sizes, cycle time, and heat fluxes for bismuth relative to water. Even under near-vacuum conditions, bismuth evaporates at a relatively high temperature when compared to water. The

**Table 10.1** Thermophysical properties of bismuth and water

Property	Bismuth	Water
Density, $\rho$ (kg/m <sup>-3</sup> )	9904.4	995
Latent heat of vaporization, $h_{lv}$ (kJ/kg)	178.9	2426
Specific volume, $v$ (m <sup>3</sup> /kg)	0.0001 (l), 327.86 (v)	0.001 (l), 29.74 (v)
Surface tension, $\sigma$ (N/m)	0.371	0.0709
Thermal conductivity, $k$ (W/mK)	13.44	0.62
Molecular weight, $M$ (kg/kmol)	208.98	18
Dynamic viscosity, $\mu$ (Pa-s)	$1.34 \times 10^{-3}$	$0.769 \times 10^{-3}$
Advancing contact angle, $\theta_{adv}$ (deg)	118.5	118.5
Receding contact angle, $\theta_{rcd}$ (deg)	101.5	101.5
Saturation temperature, $T_{sat}$ (K)	635	303
Wall temperature, $T_w$ (K)	630	298
Prandtl number (–)	0.014	5.182

degree of subcooling between the saturated vapor and the substrate is taken as 5 °C. Since the temperature interval is small, a constant thermophysical property approximation at the average temperature is utilized. At high levels of subcooling, drops are expected to form a liquid film on the substrate.

Liquid bismuth has been reported to display non-Newtonian behavior under certain circumstances. In the present work, bismuth is taken to be Newtonian with a definite viscosity for the following reason. Fluid motion in dropwise condensation is seen during (a) the instability of the liquid drop, either during its sliding motion or fall-off and (b) coalescence. Both events occur for less than 0.1% of the overall condensation cycle time. The coalescence characteristics are determined by a variety of properties such as surface tension, contact angle, density, and volume. In the context of small drops, surface tension and contact angle are central to the initial pressure difference and is unaffected by non-Newtonian behavior. Reynolds numbers during drop coalescence in the range of 400–500 may momentarily appear and non-Newtonian effects should be separately studied for this short duration. Viscosity and shear rates of bismuth in the liquid phase appear only during the late decay of the coalescence-generated velocities and during the sliding of drops over a vertical surface. They do not affect the peak velocities arising initially from inertia-surface tension coupling. Reynolds number during sliding motion can be in excess of 1000 (Sikarwar et al. 2013a, b) while Prandtl number is small (Table 10.1). The wall heat flux in the liquid metal is strongly affected by the large thermal diffusivity and is less sensitive to fluid motion. For these reasons, Newtonian fluid model for bismuth is expected to be satisfactory. Since condensation pattern and wall heat fluxes are determined by events that occur for a majority of the time, non-Newtonian behavior of bismuth has not been considered in the mathematical model.

### 10.1.1 Mathematical Modeling of Dropwise Condensation

Models of the dropwise condensation process have been reported in the literature with varying levels of approximations (Vemuri and Kim 2006; Kim and Kim 2011).

The initial mathematical model of dropwise condensation developed by the authors is described in detail elsewhere (Khandekar and Muralidhar 2014). The model proceeds from nucleation of drops to their growth and instability but treats coalescence to be an instantaneous process. The model, comprising these four steps, is schematically shown in Fig. 10.1. The model input includes nucleation site density, contact angle and hysteresis, interfacial properties, thermodynamics of phase change, and the thermophysical properties of the condensing phase. Thermophysical properties of the vapor and liquid phases are evaluated at the average of the substrate and saturation temperatures (Table 10.1). The model predicts the instantaneous condensation pattern, the mass of condensate leaving the surface, and wall heat flux. Additional quantities of interest are the cycle time of instability, liquid holdup, instantaneous and time-averaged heat fluxes, and wall shear stress. Validation studies against experiments of Rose (2002) have been discussed by the authors elsewhere (Khandekar and Muralidhar 2014; also see Chap. 3).

The instantaneous space-averaged heat transfer coefficient over an area  $A$  of the substrate during dropwise condensation is estimated in terms of the mass of the vapor condensing over the surface per unit time  $m_{avg}$  and the subcooling  $\Delta T$ . Shear

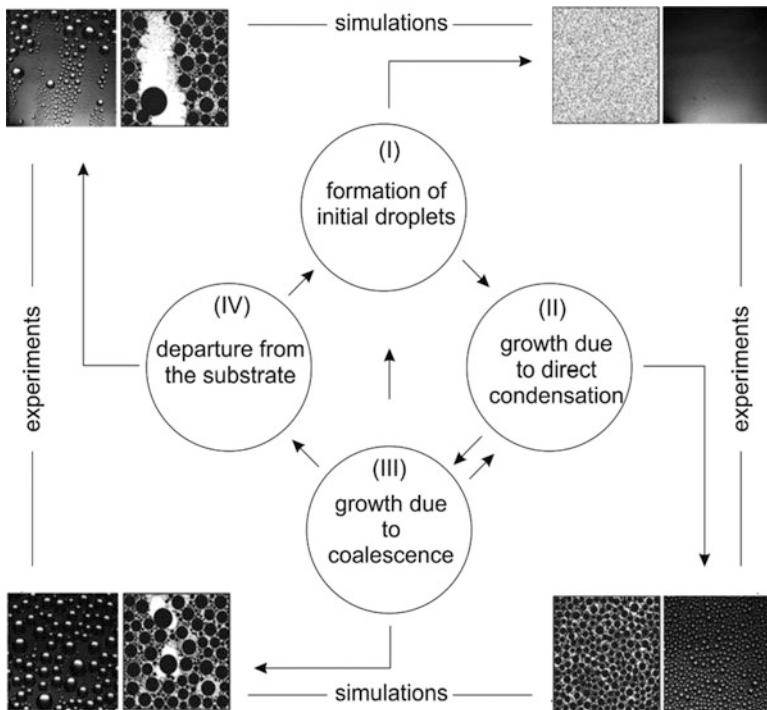


**Fig. 10.1** Schematic drawing of a mathematical model representing the dropwise condensation cycle. The model represents the condensation process in four steps, namely nucleation, growth by direct condensation of vapor, growth by droplet coalescence, and drop instability. Experimentally recorded images in water vapor (left) are shown jointly with those obtained from simulation

forces are generated by each drop when it begins to slide over the substrate. The mass of the droplet can increase during its travel on the substrate. These are discrete events and are cumulatively determined over the cycle time of condensation. The calculation of space and time-averaged shear stresses on the substrate arising from drop movement is described in Chaps. 6 and 7. The determination of wall shear stress during coalescence is described in Chap. 3.

The condensation model of the present study extends the past work of Sikarwar et al. (2013a, b) in two significant respects. First, coalescence is not treated as instantaneous. Velocity scale and timescale are estimated from non-dimensional analysis and in turn, used to estimate additional heat flux as well as the wall shear stress. Secondly, simulations are adapted to a high-performance computing system using domain decomposition that permits the use of MPI to run the computer code in parallel. The second step permits simulations over surfaces as large as  $50 \times 50$  mm in a reasonable amount of time. In addition, the choice of bismuth is novel since it is a model liquid metal with clearly prescribed thermophysical properties but has not been studied in the context of dropwise condensation.

### ***10.1.2 Scale Analysis of Drop Coalescence***

The discussion here is for the merger of two small liquid drops over textured surfaces that are hydrophobic with respect to the wetting phase. The properties of the textured surface appear in the model through the specification of the contact angle. Contact angles are a source of uncertainty in modeling dropwise condensation. Superhydrophobic surfaces with contact angles greater than  $140^\circ$  may be prepared only over small areas. For this reason, lower contact angles that, nevertheless, make the surface hydrophobic and promote dropwise condensation have been utilized in the present study.

For a horizontal surface, the equilibrium static angle is taken to be  $110^\circ$  while for a vertical surface, advancing and receding angles are  $118.5^\circ$  and  $101.5^\circ$ , respectively. These values are expected for bismuth condensation on a chemically textured copper substrate. In the condensation context, coalescence takes place over a horizontal surface in the pendant configuration. The drops are composed of the same liquid while coalescence takes place in a vapor environment. The drops are not pinned at the three-phase contact line and the footprint evolves with time. In the following discussion, scale analysis developed for a horizontal configuration is taken to be applicable for a vertical surface as well.

A large number of forces appear in the flow field with relative magnitudes that change with time. The forces can be due to surface tension, gravity, viscosity, and inertia. These primary forces are used to estimate the internal pressure of the drops. Drop size plays an important role in coalescence dynamics apart from fluid and interfacial properties. For drops of smaller volume, surface tension would be more important than inertia and gravity. Gravity forces lower internal pressure in pendant drops and hence the resulting velocities, in comparison to the sessile. In the present

**Table 10.2** Magnitudes of dimensionless parameters estimated for bismuth and water under ambient conditions. Velocity scale  $U$  is taken as  $(\sigma/\rho R)^{0.5}$ , where  $R$  is the base radius of the coalesced drop at equilibrium

Volume ( $\mu\text{L}$ ) ( $U$ , (m/s))	Base radius, (mm)	Bo	We	Fr	Re	Oh
<i>Bismuth</i>						
0.05(0.39)	0.237	$1.437 \times 10^{-3}$	1	68.130	696.034	0.015
0.5(0.27)	0.510	$0.979 \times 10^{-3}$	1	14.678	1021.640	0.068
1.5(0.22)	0.736	$0.815 \times 10^{-3}$	1	7.057	1226.920	0.142
2.5(0.20)	0.872	$0.749 \times 10^{-3}$	1	5.020	1335.960	0.199
7.5(0.17)	1.258	$0.623 \times 10^{-3}$	1	2.413	1604.400	0.414
<i>Water</i>						
0.05(0.54)	0.237	0.008	1	127.882	161.022	$0.62 \times 10^{-3}$
0.5(0.37)	0.510	0.037	1	27.551	236.348	$4.23 \times 10^{-3}$
1.5(0.31)	0.736	0.075	1	13.245	283.839	$3.52 \times 10^{-3}$
2.5(0.28)	0.872	0.106	1	9.422	309.063	$3.24 \times 10^{-3}$
7.5(0.24)	1.258	0.221	1	4.530	371.165	$2.69 \times 10^{-3}$

study, drops coalesce in vapor environment. The density difference between water and the ambient air is taken practically to be the density of the liquid. Surface tension is considered at liquid-vapor interface while a contact line force arises at the solid-liquid-vapor three-phase contact line.

The approach adopted here for scale analysis is as follows. Dimensionless parameters are defined using a pair of forces at a time, leading further to velocity and timescales. The realization of these scales in experiments is then examined. Using the experimental data as the yardstick, applicable forces during coalescence are then identified.

Instead of resolving the spatio-temporal distribution of the flow field, each regime of coalescence may be represented by its characteristic length, velocity, and time-scale. This approach is quite suitable from a modeling perspective. Coalescence is taken to introduce additional velocity, length, and timescales that are suitably incorporated in the condensation cycle. Non-dimensional quantities for equal drop volumes of bismuth and water are summarized in Table 10.2. The corresponding timescales are given in Table 10.3. The viscous-surface tension timescale is relevant closer to the instant of coalescence while viscous-inertial timescale is suggestive of the drop evolution closer to final equilibrium. The intermediate timescale (in ms) represents the appearance of large velocities jointly with significant deformation of the drop interface and is defined by a balance of inertia forces and surface tension. This timescale is of greatest interest to dropwise condensation.

**Table 10.3** Timescales estimated for coalescence of bismuth and water drops under ambient conditions; IS inertial-surface tension; VS viscous-surface tension; IV inertia-viscous

Volume( $\mu\text{L}$ )	Base radius(mm)	$t_{\text{IS}}$ (ms)	$t_{\text{VS}}$ (ms)	$t_{\text{IV}}$ (ms)
<i>Bismuth</i>				
0.05	0.237	0.595	$0.855 \times 10^{-3}$	$0.414 \times 10^3$
0.5	0.510	1.882	$1.842 \times 10^{-3}$	$1.923 \times 10^3$
1.5	0.736	3.260	$2.657 \times 10^{-3}$	$4.000 \times 10^3$
2.5	0.872	4.208	$3.150 \times 10^{-3}$	$5.622 \times 10^3$
7.5	1.258	7.289	$4.543 \times 10^{-3}$	$11.695 \times 10^3$
<i>Water</i>				
0.05	0.237	0.434	$2.70 \times 10^{-3}$	$0.070 \times 10^3$
0.5	0.510	1.374	$5.81 \times 10^{-3}$	$0.325 \times 10^3$
1.5	0.736	2.379	$8.38 \times 10^{-3}$	$0.675 \times 10^3$
2.5	0.872	3.072	$9.94 \times 10^{-3}$	$0.949 \times 10^3$
7.5	1.258	5.32	$1.43 \times 10^{-3}$	$1.975 \times 10^3$

## 10.2 Results and Discussion

Instantaneous condensation patterns of bismuth on vertical and horizontal surfaces are discussed in this chapter. Simulations on realistic meaningful surfaces are prohibitively expensive. As an alternative, simulations are carried out over substrates of increasing sizes. The sensitivity of the condensation pattern to substrate size is the examined. Condensation statistics of bismuth and water are compared.

Three parameters that strongly influence simulation are the nucleation site density, surface hydrophobicity, and the accommodation coefficient. For the present discussion, density of the nucleation sites at which liquid drops nucleate (with a radius of  $r_{\text{min}}$ ) is chosen as  $10^6 \text{ cm}^{-2}$ ; this value is quite commonly used in the condensation of water. For bismuth, nucleation site density data is surface-specific and has not been extensively tabulated. To facilitate comparison with water, this value of  $10^6 \text{ cm}^{-2}$  has been retained. The surface hydrophobicity is characterized by the equilibrium contact angle. In this context, it may be noted that fabrication of stable large-area superhydrophobic surfaces continues to be a major challenge. Such surfaces are invariably prepared by coating a substrate. Specialized coatings that make the surface superhydrophobic ( $\theta_{\text{equilibrium}} > 150^\circ$ ) tend to wear out at fairly low shear stresses and have limited shelf-life. For this reason, a hydrophobic surface with a modest equilibrium contact angle of  $110^\circ$  (hysteresis  $17^\circ$ ) has been selected for analysis. The third factor, namely the accommodation coefficient ( $\sigma$ ) determines the interfacial heat transfer coefficient. Following the discussion in the literature, values of  $\sigma = 0.05$  for water (Carey 2008) and 0.67 for bismuth (Pukha et al. 2005) have been used in the present study. Though uncertainty levels in these values is quite high, apart from their dependence on pressure, temperature, and surface



conditions, the dropwise condensation statistics are shown in later discussions of this chapter to be less sensitive to their choice.

A quantity of importance to be extracted from simulation is liquid holdup over the substrate. A larger average holdup indicates a greater heat transfer resistance and is undesirable in many applications. Similarly, a larger holdup indicates smaller productivity of the distillate and is equally undesirable. It is to be expected that the holdup would be greater for a horizontal surface compared to a vertical, being related to the cycle time and the drop size at instability. The degree of subcooling employed in simulations for bismuth as well as water is 5 K. The saturation temperature of condensing bismuth vapor is taken to be 635 K while that of water is 303 K.

Near-horizontal surfaces, with up to  $10^\circ$  inclination from the horizontal, and truly horizontal surfaces show instability mainly due to fall-off of large drops, and their respective condensation patterns were found to be indistinguishable. The results discussed in the following paragraphs use a  $10^\circ$  orientation for the near-horizontal surface but the surface, for simplicity, is addressed as horizontal.

### ***10.2.1 Condensation Patterns of Bismuth on Vertical and Horizontal Surfaces***

Spatio-temporal drop distributions, from initial nucleation to drop instability, are shown in Fig. 10.2a, b for condensation of bismuth vapor. The underside of a horizontal surface and a vertical surface are individually studied. Surface dimensions of  $10 \times 10$  mm,  $30 \times 30$  mm, and  $50 \times 50$  mm are compared. The respective images are scaled in Fig. 10.2a, b for uniformity. As a result, the size of drops on a surface of size  $50 \times 50$  mm is portrayed to be smaller than on a surface of size  $10 \times 10$  mm. Sizes of equipment of interest are larger than the dimensions studied here, but a truly multiscale simulation starting from nucleation is computationally intractable on a device scale. The approach adopted in the present work is to examine surfaces of increasing dimensions and the influence of confinement on the condensation dynamics.

The simulation begins with drops of minimum radius placed at the nucleation sites. Subsequently, they are grown over a time step by direct condensation of the surrounding vapor. Partially grown drops are coalesced with their neighbors if they touch each other. Otherwise, they continue to grow by direct condensation. Fall-off on a near-horizontal and slide-off on a vertical surface are observed if the gravitational instability criteria are fulfilled. During sliding motion, the size of the sliding drop increases by coalescence with those in its path. Instability exposes the surface to fresh nucleation and the entire cycle of nucleation to instability is resumed. When large drops merge or slide off/fall off, fresh sites are exposed, and small drops are placed at these locations. As a result, the relative population of small drops increases. Just ahead of criticality, the average drop diameter over the surface is the greatest. The combined effect of direct condensation, coalescence, and instability creates drop

horizontal

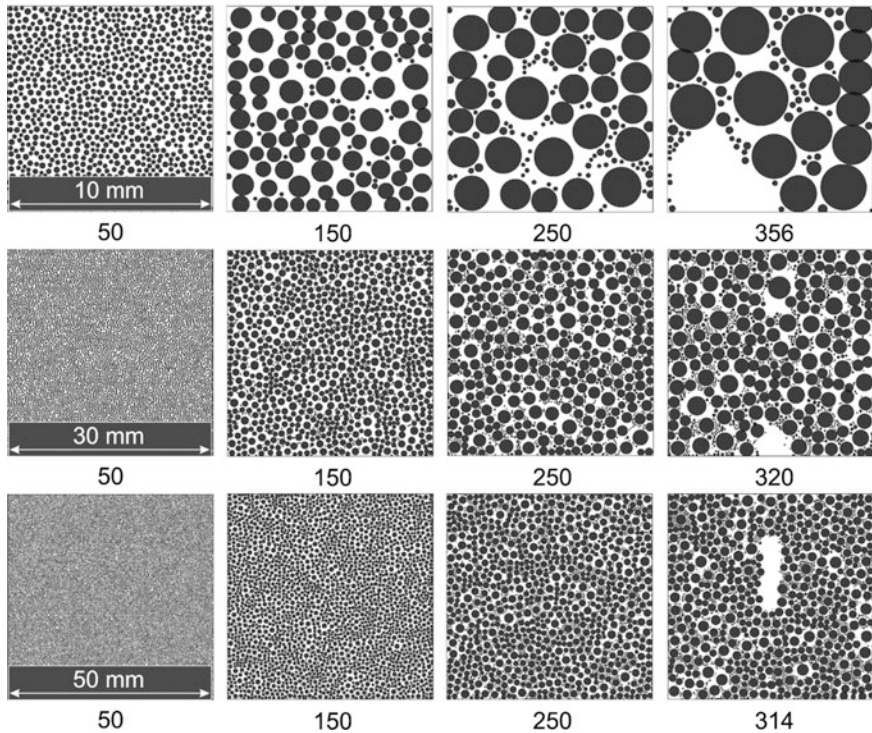


**Fig. 10.2** (a) Comparison of full surface condensation patterns of bismuth vapor over horizontal surfaces of size  $10 \times 10$  mm in the first row,  $30 \times 30$  mm in the second row,  $50 \times 50$  mm in the third. Time stamps show various stages of growth of drops and instability. The time instant of instability is seen to be insensitive to the domain size. (b) Comparison of full surface condensation patterns of bismuth vapor over vertical surfaces of size  $10 \times 10$  mm in the first row,  $30 \times 30$  mm in the second row,  $50 \times 50$  mm in the third. Time stamps show various stages of growth of drops and instability. The time instant of instability is seen to be insensitive to the domain size

population of varying sizes over the surface (Fig. 10.2a, b). These features, as discussed here, are seen in horizontal as well as vertical surfaces of the three increasing substrate sizes.

The size of a typical drop increases with time till criticality, by direct condensation and/or the coalescence process. Since the conduction resistance scales with the drop size, the relative magnitudes of conduction and convection resistance change with the drop radius, and hence with time. At any time instant, a collection of small and large drops of varying sizes prevail over the surface. Soon after instability of a large drop, the number of small drops increases due to fresh nucleation over the virgin substrate created by the movement of the unstable drop. As a part of the condensation cycle, the drop radius, and its interfacial area will increase with time. Since latent heat release and interfacial heat transfer coefficient both refer to the same

vertical

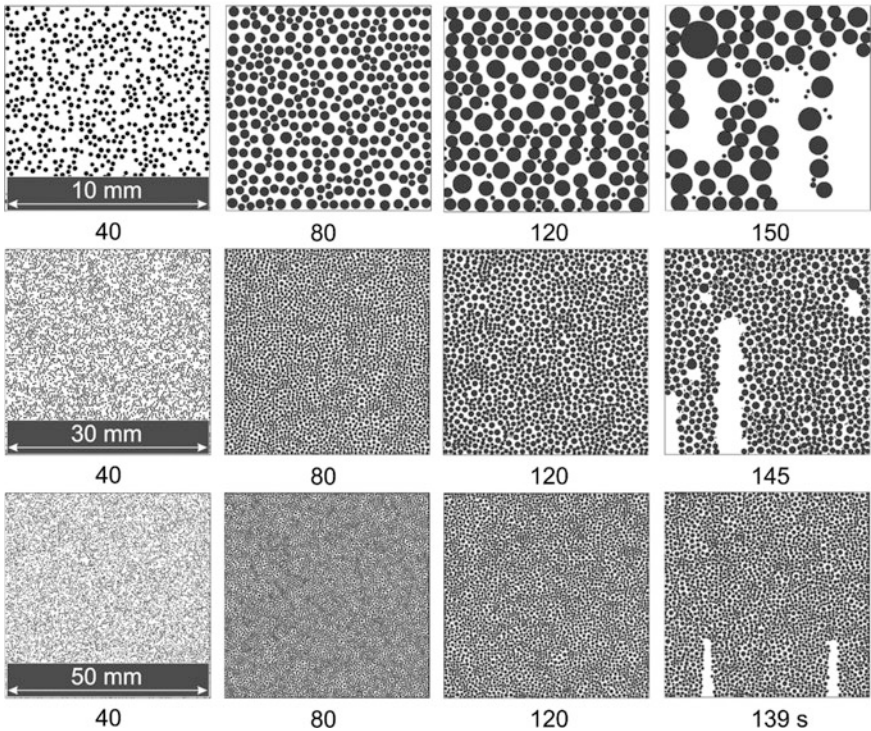


**Fig. 10.2** (continued)

vapor-liquid interface area, interfacial resistance becomes a constant, independent of the heat transfer area. In contrast, conduction resistance is small for small drops and scales with drop size. Expressions for these resistances are discussed in earlier chapters, and their numerical estimates are summarized in Table 10.4. Conduction resistance plays an important role relative to interfacial resistance in water and the total resistance changes with drops size. Thus, thermal resistance in water is minimum when the population of small drops is large and attains a maximum just before instability. For a given level of subcooling, heat flux passing through the substrate per unit time is large when the surface is populated mainly by small drops and is small when some drops have grown to greater size. Specifically, heat fluxes are large at fresh nucleation and will attain a minimum ahead of instability. In bismuth, the roles of conduction and interfacial resistances are reversed and hence, the total resistance is less sensitive to drop size.

Including finite time coalescence of drops on horizontal and vertical surfaces will further increase the wall heat flux over the value that is predicted with the assumption of instantaneous coalescence, for which the associated heat flux is zero. The coalescence event, however, lasts for a few milliseconds wherein the coalesced resultant drop grows to a finite size.

**Table 10.4** Comparison of dropwise condensation parameters of bismuth and water

		Bismuth	Water
$\theta_{\text{avg}}$ and hysteresis (degrees)		110; 17	
Nucleation site density ( $\text{cm}^{-2}$ )		$10^6$	
Subcooling, $\Delta T$ (K)		5	
Drop radius at nucleation $r_{\text{min}}$ ( $\mu\text{m}$ )		0.052	0.0035
Capillary length $r_{\text{cap}}$ (mm)		1.94	2.69
$r_{\text{max}}$ (horizontal), $r_{\text{crit}}$ (vertical) (mm)	Horizontal	2.44	3.59
	Vertical	0.6	0.878
Cycle time (s)	Horizontal	313–356	73
	Vertical	138–149	21
Radius of drop averaged over space and time, $R_{\text{avg}}$ ( $\mu\text{m}$ )	Horizontal (size of substrate) (mm $\times$ mm)	2.449 (10 $\times$ 10)	8.009 (30 $\times$ 30)
		2.199 (30 $\times$ 30)	
		2.198 (50 $\times$ 50)	
	Vertical (size of substrate) (mm $\times$ mm)	2.370 (10 $\times$ 10)	7.775 (30 $\times$ 30)
		2.368 (30 $\times$ 30)	
		2.147 (50 $\times$ 50)	
Interfacial resistance, $2/h_{\text{int}}$ ( $\text{K}\cdot\text{m}^2/\text{W}$ )		–	$51.44 \times 10^{-4}$
Conduction resistance, $(1 - \cos \theta_{\text{avg}}) R_{\text{avg}}/k$ ( $\text{K}\cdot\text{m}^2/\text{W}$ )		–	$0.00219 \times 10^{-4}$
Heat transfer coefficient averaged over space and time, $h$ ( $\text{kW}/\text{m}^2\text{K}$ ) with standard deviation	Horizontal (size of substrate) (mm $\times$ mm)	2.72; 16.8 (10 $\times$ 10)	15.88; 2.78 (30 $\times$ 30)
		3.44; 10.2 (30 $\times$ 30)	
		2.97; 6.36 (50 $\times$ 50)	
	Vertical (size of substrate) (mm $\times$ mm)	1.48; 5.27 (10 $\times$ 10)	22.8; 1.84 (30 $\times$ 30)
	2.005; 3.64 (30 $\times$ 30)		
	2.01; 2.79 (50 $\times$ 50)		

For a vertical surface, shear stresses are generated during the sliding motion of the drop. For a strictly horizontal surface, fall-off is taken to be instantaneous and shear stresses are absent. Coalescence-induced velocity generates shear stresses for both surface orientations which could be comparable or even greater than that arising from drop sliding motion.

Referring to Fig. 10.2a, b as well as Table 10.4, the size of the drop at criticality is larger for horizontal surfaces than the vertical. This is because gravity has to overcome the average contact angle for a horizontal surface while it has to overcome the advancing angle-to-receding angle difference for a vertical surface. Hence, the retention of mass is larger for a horizontal surface when compared to the vertical. It may be realized that drop growth rates are limited by the sum of conduction and vapor-liquid interfacial resistance and diminish for larger drops. In addition, since the drop grows to a larger size over a horizontal surface, the condensation cycle time is clearly greater here when compared to the vertical.

Figure 10.2a, b show that the vertical surface experiences sliding instability, as expected, for the three surfaces studied for the condensation of bismuth vapor. For a near-horizontal surface, it is mainly fall-off though a short signature of slide-off is visible for a horizontal surface of  $50 \times 50$  mm dimensions. Comparing the time instants of commencement of instability, it is seen that the surface dimensions play a role. The moment of instability is earlier on larger surfaces when compared to the smaller; it is a trend common to horizontal as well as vertical surfaces. The first instant of instability is in the range of 314–356 s for horizontal surfaces and 139–150 s for vertical surfaces over the range of dimensions considered. The proximity of the substrate boundaries is seen to stabilize large drops by limiting their growth rate, thus contributing to higher cycle times for smaller surfaces.

Condensation parameters of bismuth and water are compared in Table 10.4. Thermodynamically stable minimum radius of bismuth is 15 times greater than water. The capillary radii are of similar magnitude, showing that density and surface tension change in similar proportions. Accordingly, the maximum radius of liquid bismuth at the instant of instability for horizontal surfaces is smaller than water only by a factor of 1.5. The critical radius of bismuth at the instant of instability for vertical surfaces is smaller than water by a factor of 1.3. The average radius of a drop for bismuth during the condensation process is determined from a histogram analysis of the instantaneous condensation patterns; it is smaller for bismuth than water for horizontal and vertical surfaces by factors of 4 and 3.5, respectively.

Table 10.4 also shows that the cycle time for a vertical surface is smaller than the horizontal. Cycle time of bismuth is larger than water for horizontal and vertical surfaces by factors of five and seven, respectively. The products of density and latent heat of vaporization are similar for the two fluids. Yet, Table 10.4 shows that the heat transfer coefficient of bismuth is smaller than water for horizontal and vertical surfaces by factors of 4.6 and 11.4, respectively, for reasons discussed below.

Thermal resistance, defined as a ratio of the temperature difference and the wall heat flux at the scale of a single drop arises from conduction through the drops, and the interfacial heat transfer coefficient, the two terms appearing in series. Expressions for these resistance components for a single drop, as it evolves in time, are given in Table 10.4. For numerical evaluation and comparison, the representative radius of the drop selected is the average value that is obtained among all drops jointly evolving over the substrate within a condensation cycle. Conduction resistance, being proportional to radius, is small for a small drop and large for a large drop. It reaches a maximum value just before drop instability. A smaller cycle time will experience frequent nucleation and show a preference for smaller drops and hence a smaller overall conduction resistance. However, the interfacial resistance is a constant irrespective of the size of the drop, as noted earlier. The total thermal resistance is the sum of conduction as well as interfacial resistance which is convective in origin. In addition, the interfacial heat transfer coefficient in water is much larger than for bismuth, Table 10.4. In terms of the sum of the conduction and interfacial thermal resistance, the minimum to maximum variation for water is much greater when compared to bismuth. Accordingly, in water, one can see a strong correlation among small drop sizes, small cycle time, and large heat transfer

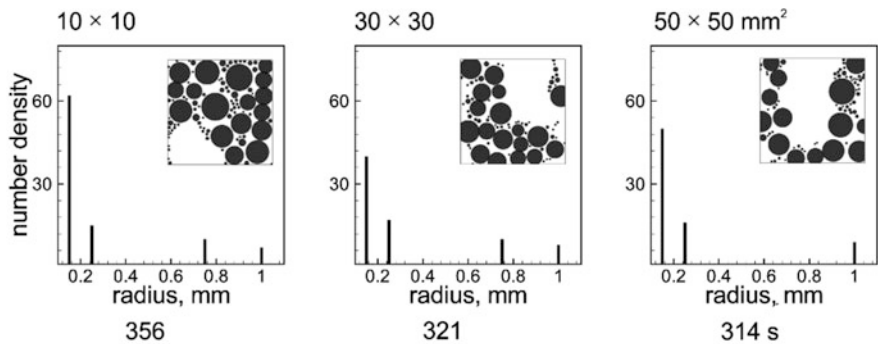


coefficient. Specifically, heat transfer coefficient for water is higher for a vertical surface when compared to the horizontal, while the average drop size is smaller.

In bismuth, interfacial resistance is certainly dominant and is a constant irrespective of the drop size. The heat transfer coefficient during bismuth condensation is smaller than in water. While the peaks attained in heat fluxes are smaller and frequent in water, Figs. 10.6 and 10.7 show strong individual peaks in heat fluxes for bismuth. Accordingly, Table 10.4 also includes the time-averaged heat transfer coefficient along with its standard deviation. In water, standard deviation in heat transfer coefficient data is small, relative to the time averaged value. However, including standard deviation in the heat transfer coefficient, such a clear difference between horizontal and vertical surfaces for bismuth condensation cannot be discerned.

Condensation patterns at the instant of instability for horizontal and vertical surfaces are shown in Fig. 10.3 for the three sizes considered. Here, the central  $10 \times 10$  mm region is extracted for discussion. These patterns are located away from the boundaries, and the question is, the extent to which the substrate size influences the condensation process at the center. Figure 10.3 also includes the time

horizontal



vertical

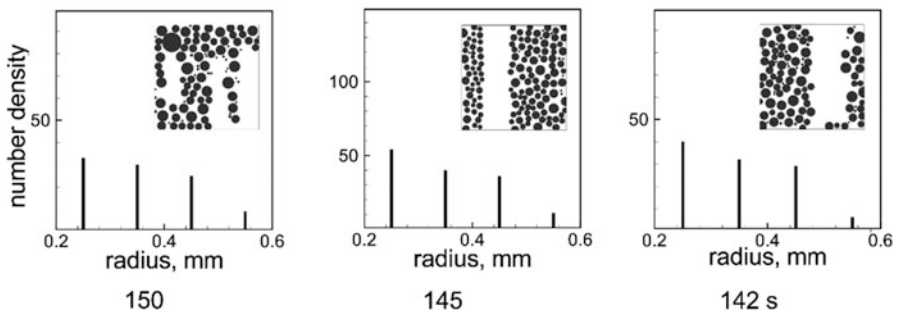


**Fig. 10.3** Comparison of condensation patterns and corresponding time for bismuth vapor at the occurrence of first instability (INSET). The number density data is shown for the central  $10 \times 10$  mm region, for the three substrate sizes ( $10 \times 10$  mm,  $30 \times 30$  mm,  $50 \times 50$  mm), both for horizontal and vertical substrates. At the onset of instability,  $r_{\max} = 2.44$  mm for horizontal substrate and  $r_{\text{crit}} = 0.6$  mm for the vertical substrate

instant of instability. For a horizontal surface, instability occurs due to droplet fall-off while it involves sliding motion for the vertical substrate. As discussed with reference to Fig. 10.2a, b, instability occurs earlier for a vertical surface as compared to the near-horizontal. The time instant of instability changes with the size of the substrate, but the influence is marginal. However, a consistent trend of boundary-induced stabilization on smaller surfaces and early instability over a larger surface are seen.

The number density distribution in terms of drop sizes at selected instants of time is shown in Fig. 10.3, where the population of small drops is often larger than that of large drops. The skewness in this ratio is smaller for a vertical surface where very large drops fall off first due to gravitational instability; this is not so for horizontal substrates. The data of Fig. 10.3, combined with the liquid holdup curves (Chap. 9) in Figs. 10.4 and 10.5, indirectly provide the number density variation with time.

Figure 10.3 also shows the drop size distribution over the surface at the moment of instability, in a number density versus radius plot. A radius interval of 0.1 mm is used for this purpose. Soon after the time instant of instability, a number of small fresh drops are nucleated. The corresponding number is very large, and the drop radii are small. The data points corresponding to very small drops are common to all the graphs and are not shown for clarity. The critical radius of instability is greater for the horizontal surface when compared to the vertical (Table 10.4), explaining the scales selected for the  $x$ -axis. For a horizontal surface, a few large drops are to be seen with the population of the largest drops ( $\sim 1$  mm) being smaller than the smallest drops ( $\sim 0.2$  mm). This trend of decreasing number density with radius is seen on all the three substrates. For a vertical surface, the pattern at instability shows

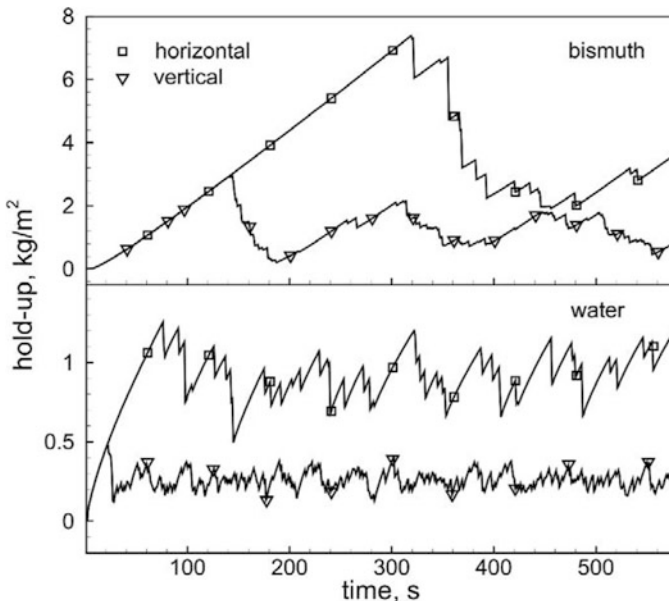


**Fig. 10.4** Variation of liquid bismuth holdup in mass units with time compared with water for a surface of size  $30 \times 30$  mm; horizontal and vertical orientations are both considered

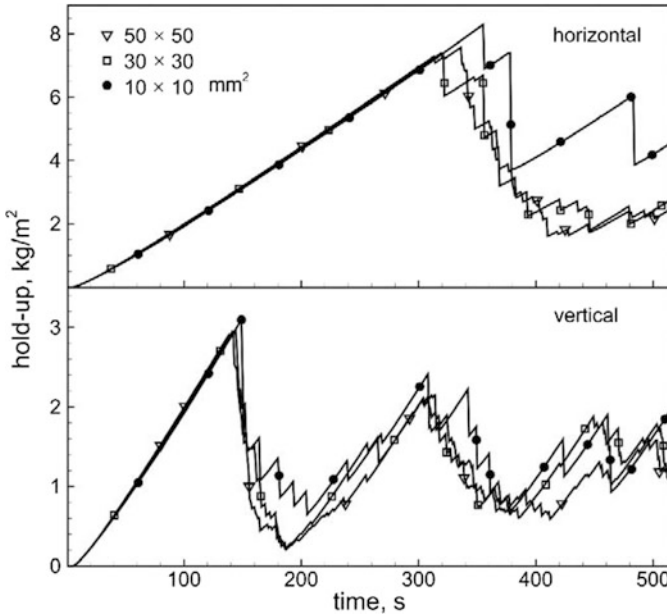


**Fig. 10.5** Variation of liquid holdup with time in bismuth for horizontal and vertical surfaces of size  $10 \times 10$  mm,  $30 \times 30$  mm,  $50 \times 50$  mm

a vertical sweep, along which, a gravitationally stable drop has been swept away. Subsequently, a large number of small nucleating drops appear. This creates a large number of drops having small radii, in contrast to large drops that are prone to instability and get eventually wiped out from the surface. Thus, the number density trend as a function of the characteristic radius has, once again, a negative slope for the vertical surface.

### 10.2.2 *Liquid Holdup*

From an application viewpoint, liquid holdup over the surface is a quantity of great importance. It is the difference between the amount of vapor condensed and the amount drained away. Since the condensate is the productive aspect of the distillation process, liquid holdup for the selected surface and inclination should be a minimum.

Instantaneous liquid holdup as a function of time is shown in Fig. 10.4. Here, bismuth is compared with water for a surface of size  $30 \times 30$  mm, for both horizontal and vertical configurations. The liquid mass staying on the surfaces increases with time, first by direct condensation and then by coalescence. At the onset of instability, large drops are drained away and the liquid holdup sharply decreases. Fresh



nucleation is then initiated and there is a gradual build-up of mass once again. There is however a well-defined average for the fluids considered.

Two major observations to emerge from Fig. 10.4 are the following. Holdup (units of  $\text{kg/m}^2$ ) on a horizontal surface is greater than the vertical surface, for both, water and bismuth. This trend makes vertical surfaces as preferred over the horizontal for condensate recovery applications. Average holdup for bismuth is larger than water by a factor of 3.8 (for horizontal) and 4.8 (for vertical). Looking at vertical and horizontal substrates individually, it is noted that the average radii of droplet are comparable for the two fluids, respectively. The condensation cycle time of water (from droplet nucleation to occurrence of instability and its repetition during dynamic steady state) for both horizontal and vertical substrates is smaller than bismuth, in conformity with the data of Table 10.4. The density ratio between bismuth and water is of the order of 10. These effects collectively explain the enhanced holdup factor of bismuth to water ( $= 4.8$ ) for vertical substrates. The average radius of a bismuth drop is smaller than water by a factor of four (Table 10.4) and correlates with the slower onset of instability and an increase in cycle time.

Variation of liquid holdup with time in bismuth for horizontal and vertical surfaces of size  $10 \times 10$  mm,  $30 \times 30$  mm, and  $50 \times 50$  mm is shown in Fig. 10.5. The plots are quite similar, indicating that the condensation cycle broadly scales over the dimensions considered. Smaller differences can, however, be detected for reasons discussed here. The average holdup is higher for a smaller surface (such as  $10 \times 10$  mm) since an unstable drop drags only a smaller fraction of liquid with it. For larger surfaces, instabilities are initiated at multiple locations and a substantial portion of the liquid condensed on the surface travels with the sliding drop. There is also an effect of the average size of the liquid drop. The drop radius influences conduction resistance and is larger for larger drops, as noted earlier. The interfacial heat transfer coefficient is not influenced by the size of the drop but is small for bismuth vapor condensing over a liquid drop. Jointly, interfacial resistance dominates conduction resistance even for large drops. The combined resistance is larger, leading to a slower growth rate on a larger surface. It leads to higher density of larger drops on the larger surface. Hence, following instability, a greater amount of liquid mass held on the surface is removed, leading to a sharper reduction in the average holdup. These details are minor, and Fig. 10.5 shows the overall effect of domain size to be marginal.

### ***10.2.3 Wall Shear Stress and Wall Heat Flux***

Apart from the condensation patterns discussed in previous sections, two other quantities of interest are the wall heat flux and wall shear stress. The surface-averaged heat flux and wall shear stress as well as local values at the coalescence sites as a function of time are presented in Figs. 10.6, 10.7, 10.8, and 10.9. The effect of the individual finite time coalescence events on the overall condensation pattern

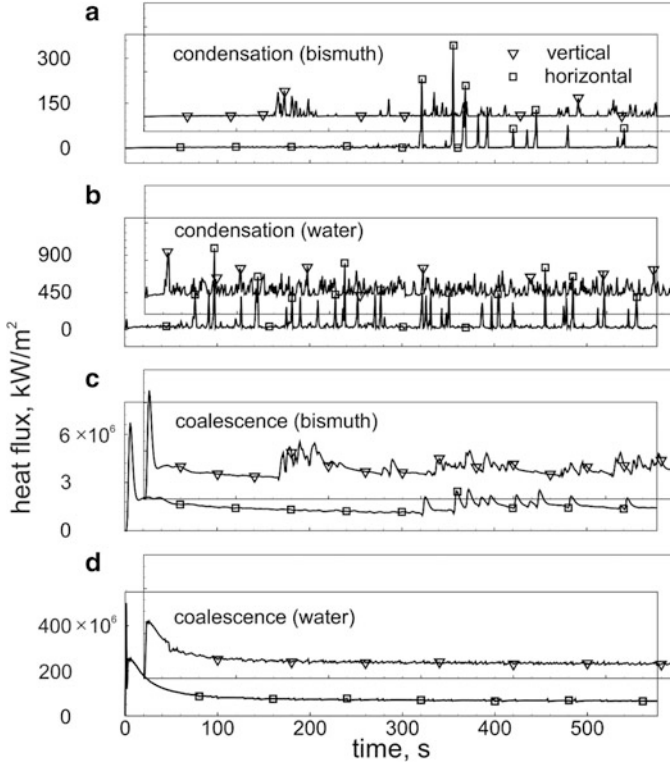


**Fig. 10.6** Variation of wall heat flux with time for horizontal and vertical surfaces of size  $30 \times 30$  mm (a) due to direct condensation in bismuth, (b) due to direct condensation in water, (c) due to coalescence in bismuth, and (d) due to coalescence in water. Note the difference in the wall heat flux scales

was found to be small. However, the fluxes and stresses during coalescence are substantial, as seen from the scales adopted in Figs. 10.6, 10.7, 10.8, and 10.9. Since the overall cycle time is of the order of minutes, a millisecond-scale coalescence process was not seen to alter the surface-averaged values. However, their magnitudes are large enough to be of concern, as discussed below.

Coalescence events occur at several sites, often simultaneously, and maximum values alone are reported in the Figs. 10.6, 10.7, 10.8, and 10.9. A total of 500 s of the condensation process is presented in the plots. In Figs. 10.6 and 10.8, bismuth is compared with water. In Figs. 10.7 and 10.9, heat flux and wall shear stress during bismuth condensation over surfaces of three different areas are compared.

Wall heat fluxes arising from (Case (i)) direct condensation (Figs. 10.6a, b and 10.7a, b) and (Case (ii)) coalescence (Figs. 10.6c, d and 10.7c) have been distinguished in the presented data. Note the scale difference in these figures in the heat flux values. Prominent and visible variability in time in the former (Case (i)) arises from drop instability where the drop size is large as it attains the critical size for

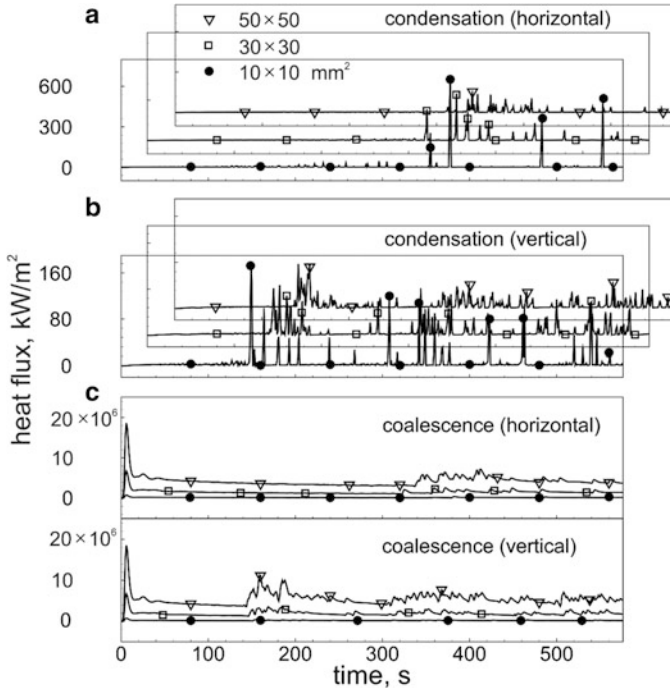


**Fig. 10.7** Variation of wall heat flux with time in bismuth for surfaces of size  $10 \times 10$  mm,  $30 \times 30$  mm,  $50 \times 50$  mm (a) due to direct condensation for horizontal orientation, (b) due to direct condensation for vertical orientation, and (d) due to coalescence for both horizontal and vertical orientation

sliding or fall off. For a horizontal surface, the drop size at fall-off instability is larger than slide-off instability of the vertical. Hence, the associated peaks in heat flux data are larger for Case (i). It is also to be emphasized that these peaks in heat flux originate primarily from a collection of nascent drops that nucleate immediately after instability of a larger drop. In Case (ii), coalescence events are spatially distributed and the extent of variability in time of the coalescence events and the resulting peak in heat flux is smaller. In general, the dropwise condensation cycle (from nucleation to instability and its periodicity) has a shorter overall time period for the vertical surface. A higher degree of variability, including coalescence, is visible as compared to the horizontal substrate.

Similar explanation can be offered for the wall shear stresses though with a difference. Wall shear is zero during the growth phase of a drop. For a horizontal surface, it is non-zero only during coalescence (Figs. 10.8a, b and 10.9a, b). For a vertical surface, it is non-zero during instability as well as coalescence. Multiple coalescence events spread over the surface give rise to a near-uniform distribution of wall shear stress. Selected peaks occurring due to drop instability arise only for the vertical surface as seen in Figs. 10.8c and 10.9c.

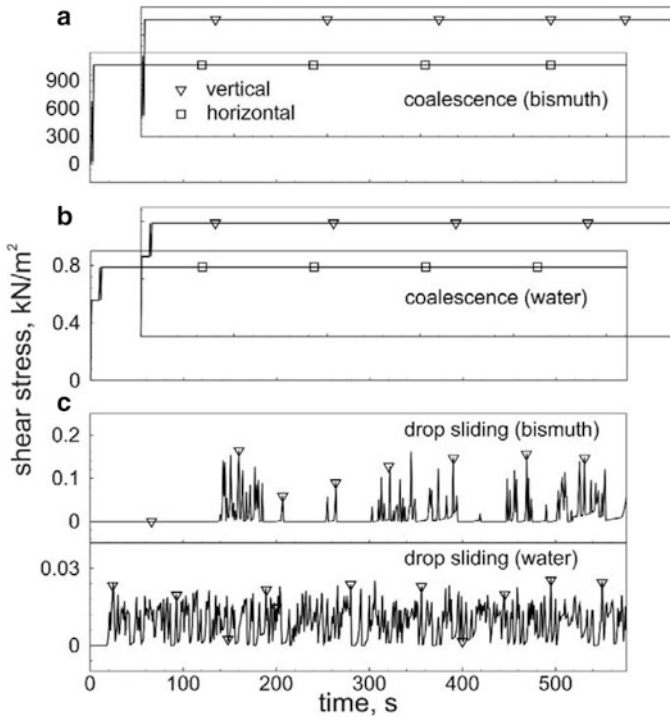


**Fig. 10.8** Variation of wall shear stress with time for surface of size  $30 \times 30$  mm (a) due to coalescence in bismuth for both horizontal and vertical orientation, (b) due to coalescence in water for both horizontal and vertical orientation, and (c) due to drop sliding for vertical orientation for bismuth and water

For a horizontal surface, a condensed drop falls off due to gravitational instability and fluid motion is restricted to the coalescence events. Hence, wall shear stress is mostly zero except for those occasional instants of time when it is large for very short time durations ( $\sim$  a few ms). For a vertical surface, wall shear is generated post drop instability when it slides down the surface. Coalescence-induced shear stress is superimposed over this value.

Textured surfaces are often coated with a promoter layer and the coating has a finite yield strength, being of the order of 38–1160 mPa (Kim et al. 2006). These yield stress values are typically applicable for organic monolayer coatings that are mainly reported in the context of condensation of water vapor. It is evident that such a coating technology on substrates, applicable for the case of water, may not withstand instantaneous shear stress values during condensation of other fluids, including metal vapor. Such coatings are prone to leaching out due to continuous cycles of condensation occurring over it, as is evident from Figs. 10.8 and 10.9. Similarly, large, though momentary, wall heat fluxes (Figs. 10.6 and 10.7) suggest thermal non-uniformity in terms of surface temperature that will affect the condensation process itself.

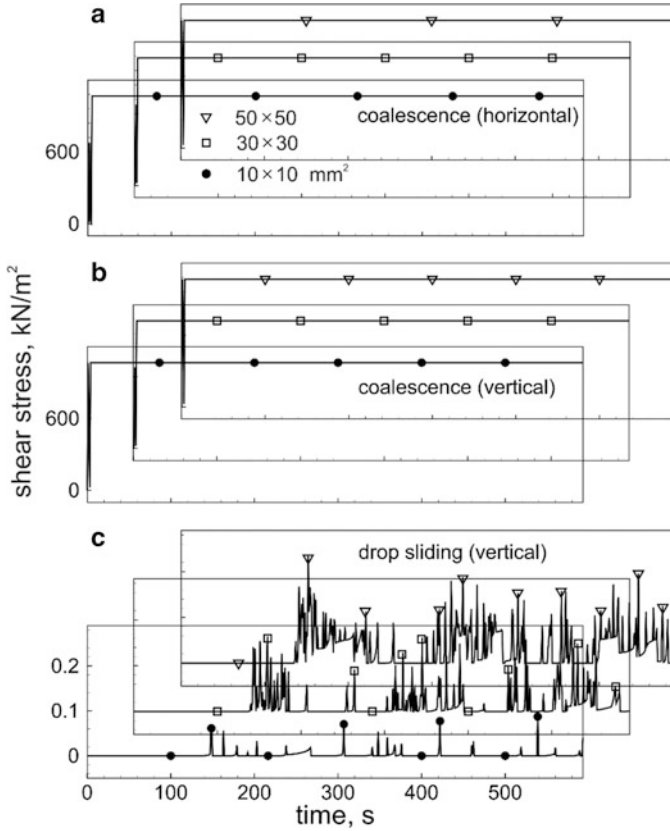


**Fig. 10.9** Variation of wall shear stress with time in bismuth for surfaces of size  $10 \times 10$  mm,  $30 \times 30$  mm,  $50 \times 50$  mm (a) due to coalescence for horizontal orientation, (b) due to coalescence for vertical orientation, and (c) due to drop sliding for vertical orientation

Direct condensation occurs at all drops, small and large from the vapor phase over the selected time step. The mass of liquid condensed over this time step multiplied by the latent heat release and divided by the sum of drop footprint areas is numerically equal to the average instantaneous wall heat flux. This is the part of heat flux associated with direct condensation. Heat flux related to coalescence arises only at those sites where two drops merge and are significant when the merging drops are physically large. Hence, the second component of heat flux is obtained by tracking coalescence events occurring at selected sites over the substrate.

Variations of wall heat fluxes with time in bismuth and water, for both horizontal and vertical surfaces of size  $30 \times 30$  mm, are shown in Fig. 10.6. Figure 10.6a, b correspond to direct condensation with the effect of local coalescence averaged out over the entire surface. Individual peaks of heat flux correspond to droplet instability. In comparison, heat flux through stationary drops is quite small and is not visible in Fig. 10.6. Peaks in wall heat flux generated due to direct condensation are seen to

be larger for a horizontal, compared to a vertical surface for both water and bismuth (Fig. 10.6a, b). Cycle time is smaller for a vertical surface compared to the horizontal, as seen in the appearance of frequent multiple peaks for water and bismuth. In addition, a larger portion of the drops is drained away from the vertical surface by sliding motion than horizontal surface during instability. Peaks in heat fluxes arise from the freshly nucleated drops, post instability. These factors combine to achieve peak heat fluxes for a horizontal surface greater than the vertical. Secondly, Fig. 10.6 shows that fluxes in water are uniformly greater than for bismuth. The product of density and latent heat of condensation for water is larger than bismuth by a factor of 1.36. Thus, latent heat is not a major reason that differentiates the wall heat flux between water and bismuth. The underlying reasons are a lower cycle time and a lower minimum drop size for water relative to bismuth, as summarized in Table 10.4. Heat fluxes arising from coalescence are reported in Fig. 10.6c, d. The peaks in water are frequent but the magnitude is smaller because of a lower Reynolds number during coalescence (Table 10.1).

Variation of wall heat flux with time in bismuth, for both horizontal and vertical surfaces of size  $10 \times 10$  mm,  $30 \times 30$  mm, and  $50 \times 50$  mm are shown in Fig. 10.7. Figure 10.7a, b provide data for direct condensation where the effect of momentary coalescence is averaged over the entire surface. The effect of surface area can be understood in the following manner. The total number of drops experiencing peak wall heat flux depends on the size of the surface. For a  $50 \times 50$  mm surface, the number of such drops undergoing instability is the greatest, while the  $10 \times 10$  mm surface has lowest number of drops simultaneously undergoing instability. Peaks in wall heat flux are seen immediately after instability. Owing to sliding motion, a vertical surface will reveal a larger number of nucleating drops. A greater portion of drops is carried away from the smaller surfaces because of sliding motion. Larger surfaces may have instability at multiple locations and yet, a smaller portion of the drops will be drained away. Peaks in wall heat flux based on direct condensation, as well as coalescence, are proportional to this fractional number undergoing instability. Hence, larger fluctuations are seen on smaller surfaces than the larger surfaces for both horizontal and vertical configurations.

Wall heat fluxes generated during coalescence of drops of bismuth are shown in the Fig. 10.7c. For horizontal surfaces of sizes  $10 \times 10$  mm,  $30 \times 30$  mm, and  $50 \times 50$  mm, these values are  $0.16 \times 10^6$  kW/m<sup>2</sup>,  $1.64 \times 10^6$ , and  $4.86 \times 10^6$  kW/m<sup>2</sup>, respectively. Average values of wall heat flux generated during coalescence of drops of bismuth on the three vertical surfaces are  $0.24 \times 10^6$  kW/m<sup>2</sup>,  $2.3 \times 10^6$  kW/m<sup>2</sup>, and  $6.77 \times 10^6$  kW/m<sup>2</sup>, respectively. Wall heat flux, both based on direct condensation and coalescence, shows increasing trends with an increase in surface area though the differences are small. As discussed in the context of Fig. 10.6, peak wall fluxes for direct condensation are greater for horizontal surfaces compared to the vertical. Orientation does not affect the coalescence fluxes significantly (Fig. 10.7). It is also seen that frequent coalescence peaks are seen on larger surfaces as compared to the smaller ones. Coalescence-related heat fluxes show momentary large peaks. However, the drop footprint is small and their contribution to the

cumulative surface-averaged value of the net heat flux is small. Thus, the average value of the heat flux is principally governed by the direct vapor condensation process over the substrate.

Variation of wall shear stress with time in bismuth and water for both horizontal and vertical surfaces of size  $30 \times 30$  mm is shown in Fig. 10.8. The instantaneous wall shear stress induced during coalescence of any two pair of droplets is estimated using centroidal analysis of Chap. 3. It is multiplied by the footprint area of the coalesced drop. At any instant of time, several such pairs may be coalescing on the substrate. The net shear force generated due to all such occurrences of coalescence events divided by the footprint area of all coalesced drops yield the average shear stress contribution due to droplet coalescence. This data is reported in Fig. 10.8a, b for bismuth and water, respectively.

The effect of substrate size on wall shear stress is shown in Fig. 10.9 for bismuth. Substrate areas,  $10 \times 10$  mm,  $30 \times 30$  mm, and  $50 \times 50$  mm, respectively, are considered. Figure 10.9a, b correspond to wall shear stresses generated during coalescence. These values are, in general, quite large, because they are associated with a small area under the coalescing drops. Since the coalescence events are spatially distributed, wall shear stress associated with coalescence for the substrate as a whole is nearly constant in time (both in Figs. 10.8a, b and 10.9a, b).

Figures 10.8c and 10.9c present data for shear stresses generated during the sliding motion of individual droplets after they become unstable over a vertical substrate. This computation is carried out from a numerically determined Reynolds number correlation described in the previous work of the authors (Khandekar and Muralidhar 2014). For a horizontal surface, this contribution to shear stress is zero as unstable drops do not slide but actually fall off from the substrate. For vertical surfaces, sliding velocities which are generated are usually small, the drop size continues to become larger as the sliding drop gains mass. The process is infrequent relative to coalescence. Hence, surface-averaged wall shear stress due to sliding motion of unstable drops is substantially smaller than the coalescence-based wall shear stress. Instability events are more frequent in water when compared to bismuth, as seen in cycle times listed in Table 10.4. Accordingly, a larger number of momentary peaks are visible for water (Fig. 10.8c). For coalescence as well as in sliding motion, the shear stress generated in water is much smaller than bismuth, a result that follows from a larger dynamic viscosity of bismuth. From Fig. 10.9c, it is also noted that at instability, drops on larger vertical surfaces have to travel a longer distance than a smaller surface. Hence, shear prevails for a longer duration, generating larger wall shear stresses on larger surfaces. The maximum wall shear stress induced during sliding of drops on vertical surfaces of sizes  $10 \times 10$  mm,  $30 \times 30$  mm,  $50 \times 50$  mm are  $0.1 \text{ kW/m}^2$ ,  $0.16 \text{ kW/m}^2$ ,  $0.23 \text{ kW/m}^2$ , respectively. Thus, wall shear stresses based on drop sliding show an increasing trend with an increase in surface area though the differences are small.

Coalescence-based wall shear stress is directly proportional to characteristic velocity and dynamic viscosity and inversely proportional to the base radius. Estimated velocity for bismuth is larger than in water by a factor of 1.44 and the

average radius of a bismuth drop is smaller than water by a factor of 4 (Table 10.4). Viscosity of bismuth is larger than water by a factor of 175 (Table 10.1). These parameters combine to generate larger wall shear stress in bismuth relative to water. During sliding motion, bismuth drops acquire a much higher terminal velocity (Table 10.2) and accordingly, shear stresses are again higher, relative to water.

### 10.3 Closure

A hierarchical model of dropwise condensation described in Chaps. 6 and 7 has been extended by including the details of droplet coalescence dynamics. The process starts from direct condensation at nucleation sites over the cold substrate. It is followed by growth arising from direct condensation as well as coalescence and slide off or fall off due to gravity, depending on the substrate orientation. The process is cyclic and spatially distributed over the substrate. Quantities of interest, including instantaneous condensation patterns, wall shear stress, and wall heat flux, have been predicted. Characteristic velocity and timescales of coalescence determined using scale analysis are used to extend the condensation model and determine local wall shear stresses and heat transfer rates. The present work reports data related to condensation of bismuth vapor underneath a near-horizontal surface and on a vertical surface. These are further compared with the condensation of water vapor on a hydrophobic surface. Changes in condensation parameters with the overall surface area of the substrate are investigated. Instantaneous wall heat fluxes and shear stresses arising from coalescence events are seen to be substantial. However, the surface and time-averaged heat flux data is barely affected. Similarly, wall shear stress data is only marginally influenced. However, large instantaneous shear stresses have a significant impact on the life of the coated surface and should be considered in analysis.

Relative to water, liquid bismuth has a higher density, higher thermal conductivity, higher surface tension with vapor, higher viscosity but a much smaller latent heat of vaporization, thus generating several contrasts with it. Cycle time, minimum radius of drop, holdup, and vapor-liquid interfacial resistance of liquid bismuth are larger than water for both horizontal and vertical surfaces. Maximum radius of drop, average radius of drop, conductance resistance, and average heat transfer coefficient of liquid bismuth are smaller than water for both horizontal and vertical surfaces. As a result, wall heat flux based on direct condensation as well as coalescence is substantially larger for water than liquid bismuth for both horizontal and vertical surfaces. The average heat transfer coefficient in bismuth is smaller than for water. Fluctuations in heat fluxes in water are small but frequent while in bismuth, the local peaks arising from drop instability are larger and occasional. Wall shear stresses generated during coalescence as well as sliding of drops are larger for liquid bismuth than water for both horizontal and vertical surfaces.